Three-dimensional reconstruction of root cells and interdental cells in the rat inner ear by serial section scanning electron microscopy

Ryusuke Shodo[1,2], Manabu Hayatsu[1], Daisuke Koga[3], Arata Horii[2], and Tatsuo Ushiki[1]

[1]Division of Microscopic Anatomy, Niigata University Graduate School of Medical and Dental Sciences, Niigata, Japan; [2]Department of Otolaryngology Head and Neck Surgery, Niigata University Graduate School of Medical and Dental Sciences, Niigata, Japan; and [3]Department of Microscopic Anatomy and Cell Biology, Asahikawa Medical University, Asahikawa, Japan

ABSTRACT

In the cochlea, a high K^+ environment in the endolymph is essential for the maintenance of normal hearing function, and the transport of K^+ ions through gap junctions of the cochlear epithelium is thought to play an important role in endolymphatic homeostasis. The aim of the present study was to demonstrate the three-dimensional (3D) ultrastructure of spiral ligament root cells and interdental cells, which are located at both ends of the gap junction system of the cochlea epithelium. Serial semi-thin sections of plastic-embedded rat cochlea were mounted on glass slides, stained with uranyl acetate and lead citrate, and observed by scanning electron microscopy (SEM) using the backscattered electron (BSE) mode. 3D reconstruction of BSE images of serial sections revealed that the root cells were linked together to form a branched structure like an elaborate “tree root” in the spiral ligament. The interdental cells were also connected to each other, forming a comb-shaped cellular network with a number of cellular strands in the spiral limbus. Furthermore, TEM studies of ultra-thin sections revealed the rich presence of gap junctions in both root cells and interdental cells. These findings suggest the possibility that both root cells and interdental cells contribute to K^+ circulation as the end portion of the epithelial cell gap junction system of the cochlea.

INTRODUCTION

The mammalian cochlea has two unique compartments filled with endolymph and perilymph. For the conversion of an acoustic stimulus into an electrical signal, high K^+ and highly positive-potential environments are essential in the endolymph (4, 12, 13), because hair cell depolarization in the organ of Corti is produced by the flow of K^+ into the hair cells. K^+ is then promptly released into the extracellular space at the basolateral site of the hair cell (18) and is incorporated into the supporting cells (30). Next, K^+ in the supporting cells is most likely recycled back to endolymph by several different mechanisms to maintain a high K^+ environment in the endolymph.

Previous studies using freeze-fracture electron microscopy have shown the presence of gap junctions in supporting cells, which suggests that communication occurs between these cells (9, 17, 31). Kikuchi et al. (20) further studied the distribution of gap junctions in the cochlea by both immunohistochemistry and transmission electron microscopy (TEM) and identified the importance of K^+ transport through cell-to-cell gap junctions in endolymph homeostasis. This research suggested the presence of two independent gap junction systems: the “epithelial cell gap junction system” and the “connective tissue gap junction system.” The epithelial cell gap junction system contains spiral ligament root cells, outer sulcus cells, supporting cells (of the organ of Corti), inner sulcus cells, and interdental cells, whereas the connective tissue gap junction system is composed of fibrocytes of the

spiral ligament, basal cells and intermediate cells of the stria vascularis, and fibrocytes of the spiral limbus. Since then, many researchers have been interested in the localization of connexin subtypes (e.g., connexin 26, 30, 31, and 43) in the inner ear (1, 8, 15, 23, 27). The existence of hearing loss diseases that are caused by mutations of these connexin genes also supports the critical importance of K^+ circulation through gap junctions in normal hearing (3, 19, 26, 29).

Because root cells and interdental cells are located at both ends of the epithelial cell gap junction system and are found in close proximity to the connective tissue gap junction system, these cells are considered to play an important role in K^+ circulation by delivering K^+ from the epithelial cell gap junction system to the connective tissue one. However, the structure of these cells has not been fully investigated in relation to their three-dimensional (3D) arrangement. Thus, the aim of this study was to clarify the 3D arrangement of root cells and interdental cells through the 3D reconstruction of semi-thin serial sections by scanning electron microscopy (SEM) using the backscattered electron (BSE) mode. We also investigated the presence of gap junctions in these cells by transmission electron microscopy (TEM).

MATERIALS AND METHODS

Animals

Male Wistar rats, 8 to 10 weeks of age, were used in our study. This study was performed with the approval of the Ethics Committee for Animal Experimentation at Niigata University (No. 209-2).

Serial section SEM (SS-SEM)

Under deep anesthesia with pentobarbital sodium (0.13mg/g) the animals were perfused through the heart with a physiological saline followed by a mixture of 2% paraformaldehyde and 2.5% glutaraldehyde in 0.1M phosphate buffer (pH 7.4). After perfusion fixation, the temporal bones were rapidly removed from the body and the tympanic bullae were opened with forceps. In order to expose the cochlear duct, the round window was perforated, the stapes was removed, and the bone wall of the cochlear apex was partially removed under a dissecting microscope. These dissected tissues were immersed again in the same fixative for at least 24 h at 4°C.

Samples were decalcified in 10% ethylenediamine tetraacetic acid (EDTA) in 0.1M phosphate buffer (pH 7.4) according to a modification of the microwave-accelerated method (10). Briefly, the specimens were immersed in a glass beaker containing 200 mL of the EDTA solution, which was then placed in an ice bath, and intermittently irradiated at 300 W using a microwave processor (MI-77, Azumaya Ika Kikai, Tokyo, Japan) at a temperature below 40°C. Microwave irradiation was performed for 6 h per day, and the solution was stirred gently at about 20°C when not being subjected to irradiation. The EDTA solution was changed daily and the total treatment time was 2–3 days. All decalcified specimens were post-fixed using a modification of the ferrocyanide-reduced osmium method (37), by treating with 2% osmium tetroxide containing 1.5% potassium ferrocyanide for 3 h at about 20°C. The specimens were then dehydrated through a graded series of ethanol and embedded in Epon 812. Semi-thin sections at 0.5-µm thickness were serially cut with a diamond knife, mounted on glass slides, stained with toluidine blue, and observed with a light microscope (DP80, Olympus, Tokyo, Japan).

For SEM, the toluidine blue-stained sections were further stained with uranyl acetate for 10 min and lead citrate for 5 min. Glass slides of the sections were cut into small pieces, mounted on

aluminum stubs with conductive tape, coated with platinum-palladium (1-nm thick) by using an ion-coater (MSP-10, Vacuum Device Co. Ltd., Ibaraki, Japan), and observed in a scanning electron microscope (SU3500, Hitachi, Tokyo, Japan) at an accelerating voltage of 5 kV. BSE images were obtained with a highly sensitive, annular BSE detector. The positions and boundary inclinations of serial section images, reversed in black-and-white contrast, were adjusted with Delta Viewer (a freeware program for Macintosh available on the internet; Wada M, Osaka, Japan), arbitrary lesions were selected with Adobe Photoshop CS (Adobe, CA, USA), and 3D reconstruction was performed with Amira 5 (Maxnet, Tokyo, Japan) using a personal computer.

Transmission electron microscopy (TEM).

The specimens fixed above were embedded in Epon 812 using the same procedure as SS-SEM. Ultra-thin sections at a thickness of 70 nm were cut, placed on 150-mesh copper grids, stained with uranyl acetate (for 10 min) and lead citrate (for 5 min), and observed under a transmission electron microscope (H-7650, Hitachi, Tokyo, Japan) at an accelerating voltage of 80 kV.

RESULTS

Light microscopy and BSE-mode SEM

Light microscopy of toluidine blue-stained semi-thin sections was useful for observing the entire shape of the cochlea (Fig. 1a). The top, middle, and basal turns of the cochlear duct were determined in the cross-section images along the modiolus. Reissner's membrane, tectorial membrane, organ of Corti, spiral limbus, spiral ligament, and stria vascularis, as well as hair cells and supporting cells (i.e., Deiters cells, pillar cells, Hensen's cells, Claudius cells, inner sulcus cells, and outer sulcus cells) were also identified at higher magnification. However, the shape of interdental cells of the spiral limbus and root cells were not clear by light microscopy (Fig. 1b, c).

After observation by light microscopy, the semi-thin sections were observed by BSE-mode SEM (Fig. 1a´-c´). Because BSE-mode SEM is more useful for observing semi-thin sections at higher magnification than light microscopy (Fig. 1a´), the hair cells and supporting cells in the organ of Corti, as well as the outer sulcus, the spiral ligament, and the stria vascularis, were more clearly observed at the high magnification of SEM images.

Outer sulcus cells were characterized by a darkly staining cytoplasm and appeared to extend their processes into the spiral ligament, showing a connection to the root cells (Fig. 1b´). Although the shape of fibrocytes in the spiral ligament was not clear by BSE-made SEM, the shape of the root cells was clearly determined because of their bright cytoplasm. These root cells were connected to each other to form a large, branched cellular mass in the spiral ligament, as if it were elaborately branched like a tree root (pink-colored cellular mass in Fig. 2a–f).

Observations of the inner sulcus and spiral limbus by BSE-mode SEM (Fig. 1c´) revealed that inner sulcus cells had a bright cytoplasm and were lined on the surface of the inner sulcus. Some inner sulcus cells were connected to strands of interdental cells in certain regions. Each cellular strand consisted of a number of interdental cells and ran parallel to each other toward the surface facing the tectorial membrane. The interdental cells on the top surface then extended their processes to make a plate-like structure. At the inner end of the spiral limbus, the interdental cells were connected to cells of the Reissner's membrane (Fig. 3a–f).

3D reconstruction of root cells

After obtaining BSE images of 120 semi-thin serial sections by SEM, the positions and inclinations of black-and-white reversed images were adjusted, and arbitrary lesions were selected using a personal computer (Fig. 2a–f). 3D reconstruction of root cells and outer sulcus cells showed that root cells, together with outer sulcus cells, were connected to each other to form an elaborately branched cell mass, the shape of which is similar to that of a tree root (Fig. 2g–i). The nuclei of the cell column were concentrated toward the outer sulcus side.

3D reconstruction of interdental cells

3D reconstruction of interdental cells and inner sulcus cells was made from 120 serial sections (Fig. 3a–f). The interdental cells in the inner side near Reissner's membrane were spherically shaped and connected to each other to form a single layer facing the tectorial membrane. The interdental cells in the outer side near the vestibular lip were elongated and extended their plate-like processes toward the surface to form a continuous plate that faced toward the tectorial membrane. The interdental cells in this portion also formed several cellular strands by connecting to interdental cells in line. These interdental cell strands were also connected to inner sulcus cells. Thus, the interdental cells and the inner sulcus cells formed a comb-shaped cellular network in the spiral limbus (Fig. 3g–j).

Transmission electron microscopy (TEM)

In the spiral ligament, the cell membranes and organelles of root cells were clearly detected by TEM (Fig. 4a–c). The root cells had oval nuclei, many mitochondria, and irregular membranes that interdigitated with adjacent cells (Fig. 4a). At higher magnification, gap junctions were observed in the areas between the root cells (Fig. 4b, c).

Similar findings were also confirmed in the interdental cells of the spiral limbs (Fig. 5a–c). The interdental cells had oval nuclei with irregular membranes that interdigitated with each other (Fig. 5a). Gap junctions were also observed between these membrane interdigitations (Fig. 5b, c). Adherent junctions were also found between the plate-like processes facing the tectorial membrane.

DISCUSSION

In the present study, we attempted to elucidate the 3D architecture of root cells and interdental cells in the rat cochlea by performing 3D reconstruction of BSE images obtained from serial semi-thin sections by SEM. We also observed these cells by TEM and confirmed the presence of gap junctions in these cells. Thus, we succeeded in demonstrating the entire 3D shape of the root cell mass and interdental cell mass – the part of the epithelial gap junction system in the cochlea responsible for K^+ maintenance of the endolymph.

Root cells

The specific form of root cells was first reported in the 19th century, and these cells were considered to be the key component connecting the sensory epithelium in the cochlear lateral wall. Lawrence (24) observed the cochlea of rhesus monkeys by light microscopy and showed how root cells had stretched out the cytoplasmic processes located at the lower region of the spiral ligament. Duvall (6) observed the outer sulcus and the root cells of guinea pigs by TEM, showing that the root cells formed branched bundles. Additional TEM studies also revealed the ultrastructure of root cells (7,

34), but few studies have focused on the 3D architecture of root cells, except a study by Jagger et al. (16), in which a dye was injected into root cells to demonstrate their spread.

Our 3D reconstruction studies revealed that a number of root cells connect with each other to form a branched cell mass, similar in shape to a tree root. These elaborate branches were found to be buried in the spiral ligament, where type II fibrocytes were also shown to be distributed over the inferior region of the cochlear lateral wall (33). Because the hypothesis that K^+ circulation is directed from the outer hair cells to the cochlear lateral wall is generally accepted, K^+ is thought to be transported through gap junctions located between epithelial cells, according to its concentration gradient. Previous studies also revealed the presence of Na^+, K^+-ATPase and Na^+-K^+-Cl^- cotransporters in type II fibrocytes, which probably act as a driving force that produces concentration gradients (5, 14, 28, 32, 33). These findings suggest that the elaborate branches of the root cell mass may play an important role in transporting K^+ to type II fibrocytes. The large surface area of root cells may be necessary for efficient K^+ circulation (Fig. 6).

Liu and Zhao (27) determined the expression of connexin 26 and 30 on the root cells of the rat cochlear, whereas Liu et al. (26) showed that expression of connexin 43 on the root cells of the mouse cochlea. Our preliminarily immunohistiochemistry studies showed that connexin 26 and 30 are expressed in the rat epithelial gap junction system, except in root cells. Further studies are needed to clarify this expression pattern.

Interdental cells

Previous research results suggest that interdental cells function as anchoring cells (11) as well as secretory cells of the tectorial membrane (2). In addition to TEM-based morphological analysis (25, 36), Spicer and Schulte (35) categorized interdental cells into three groups based on their localization: lateral, central, and medial interdental cells. Our 3D reconstruction studies of interdental cells revealed that all interdental cells are connected to each other, forming a continuous cell network in the spiral limbus. The presence of gap junctions in this cellular network suggests that this portion also acts as the end of the epithelial cell gap junction system for K^+ transport (Fig. 6).

Few studies have examined K^+ circulation from the inner hair cells, while K^+ circulation from the outer hair cells is better understood. Our plausible hypothesis to consider is that K^+ incorporated in the inner hair cells is circulated to the endolymph, though its specific route has not been clearly determined. Spicer and Schulte (35) claimed the presence of an “inside route” (through the border cells, the inner sulcus cells, and the interdental cells) and suggested the possibility that the Na^+, K^+-ATPase of the interdental cells functions as a driving force. Further research confirming this “inside route” is required; however, the continuous network of interdental cells demonstrated in this study is consistent with the possibility this functional route.

Serial section SEM

Here, we performed BSE imaging of plastic-embedded semi-thin sections on glass slides by SEM, which allowed us to examine the ultrastructure of the cochlea. These images are similar to classical TEM images of ultrathin sections but can be compared to light micrographs of the same portions after staining the sections with toluidine blue. This technique is useful for observing wide areas of the sections without any obstructions in view, such as the TEM specimen grid (21).

Previously, our group also reported the 3D reconstruction of the Golgi apparatus by using BSE images of serial ultrathin sections obtained from SEM (22). Here, we applied this technique to

serial semi-thin section studies to analyze the 3D arrangement of cellular components in the rat cochlea. We thus showed that this technique is useful for visualizing the 3D arrangement of root cells and interdental cells, even though these cells are surrounded and embedded in the connective tissue components of the spiral ligament and the spiral limbus. Thus, this technique has great potential in examining various cell components, allowing for 3D reconstruction of a wide range of cells and tissues.

CONCLUSIONS

The present study demonstrated the ultrastructure of root cells and interdental cells and showed the 3D arrangement of these cells via the 3D reconstruction of BSE images obtained from serial semi-thin sections by SEM. In the 3D reconstructed images, the root cells were linked together to form a branched structure, similar to a tree root in the spiral ligament. The interdental cells were also connected to each other to form a comb-shaped cellular network in the spiral limbus. TEM studies revealed the presence of gap junctions in both the root cells and in the interdental cells. These findings strongly suggest that both root cells and interdental cells contribute to K^+ circulation as the end portion of the epithelial cell gap junction system of the cochlea.

REFERENCES

1. Ahmad S, Chen S, Sun J and Lin X (2003) Connexins 26 and 30 are co-assembled to form gap junctions in the cochlea of mice. *Biochem Biophys Res Commun* **307**, 362–368.
2. Belanger LF (1953) Autoradiographic detection of S35 in the membranes of the inner ear of the rat. *Science* **118**, 520–521.
3. del Castillo I, Villamar M, Moreno-Pelayo MA, del Castillo FJ, Alvarez A, Tellería D, Menéndez I and Moreno F (2002) A deletion involving the connexin 30 gene in nonsyndromic hearing impairment. *N Engl J Med* **346**, 243–249.
4. Corey DP and Hudspeth AJ (1979) Ionic basis of the receptor potential in a vertebrate hair cell. *Nature* **281**, 675–677.
5. Crouch JJ, Sakaguchi N, Lytle C and Schulte BA (1997) Immunohistochemical localization of the Na-K-Cl co-transporter (NKCC1) in the gerbil inner ear. *J Histochem Cytochem* **45**, 773–778.
6. Duvall AJ 3rd (1969) The ultrastructure of the external sulcus in the guinea pig cochlear duct. *Laryngoscope* **79**, 1–29.
7. Galić M and Giebel W (1989) An electron microscopic study of the function of the root cells in the external spiral sulcus of the cochlea. *Acta Otolaryngol Suppl* **461**, 1–15.
8. García Berrocal JR, Méndez-Benegassi I, Martí C and Ramírez Camacho R (2008) Intervention of spiral ligament fibrocytes in the metabolic regulation of the inner ear. *Acta Otorrinolaringol Esp* **59**, 494–499.
9. Gulley RL and Reese TS (1976) Intercellular junctions in the reticular lamina of the organ of Corti. *J Neurocytol* **5**, 479–507.
10. Hellström S and Nilsson M (1992) The microwave oven in temporal bone research. *Acta Otolaryngol Suppl* **493**, 15–18.
11. Hilding AC (1952) Studies on the otic labyrinth. On the origin and insertion of the tectorial membrane. *Ann Otol Rhinol Laryngol* **61**, 354–370.

12. Hudspeth AJ and Corey DP (1977) Sensitivity, polarity, and conductance change in the response of vertebrate hair cells to controlled mechanical stimuli. *Proc Natl Acad Sci USA* **74**, 2407–2411.
13. Hudspeth AJ and Jacobs R (1979) Stereocilia mediate transduction in vertebrate hair cells (auditory system/cilium/vestibular system). *Proc Natl Acad Sci USA* **76**, 1506–1509.
14. Ichimiya I, Adams JC and Kimura RS (1994) Immunolocalization of Na^{+}, K^{+}-ATPase, Ca^{++}-ATPase, calcium-binding proteins, and carbonic anhydrase in the guinea pig inner ear. *Acta Otolaryngol* **114**, 167–176.
15. Jagger DJ and Forge A (2006) Compartmentalized and signal-selective gap junctional coupling in the hearing cochlea. *J Neurosci* **26**, 1260–1268.
16. Jagger DJ, Nevill G and Forge A (2010) The Membrane Properties of Cochlear Root Cells are Consistent with Roles in Potassium Recirculation and Spatial Buffering. *J Assoc Res Otolaryngol* **11**, 435–448.
17. Jahnke K (1975) The fine structure of freeze-fractured intercellular junctions in the guinea pig inner ear. *Acta Otolaryngol Suppl* **336**, 1–40.
18. Johnstone BM, Patuzzi R, Syka J and Syková E (1989) Stimulus-related potassium changes in the organ of Corti of guinea-pig. *J Physiol* **408**, 77–92.
19. Kelsell DP, Dunlop J, Stevens HP, Lench NJ, Liang JN, Parry G, Mueller RF and Leigh IM (1997) Connexin 26 mutations in hereditary non-syndromic sensorineural deafness. *Nature* **387**, 80–83.
20. Kikuchi T, Kimura RS, Paul DL and Adams JC (1995) Gap junctions in the rat cochlea: immunohistochemical and ultrastructural analysis. *Anat Embryol (Berl)* **191**, 101–118.
21. Koga D, Kusumi S, Shodo R, Dan Y and Ushiki T (2015) High-resolution imaging by scanning electron microscopy of semithin sections in correlation with light microscopy. *Microscopy* **64**, 387–394.
22. Koga D, Kusumi S and Ushiki T (2016) Three-dimensional shape of the Golgi apparatus in different cell types: serial section scanning electron microscopy of the osmium-impregnated Golgi apparatus. *Microscopy* **65**, 145–157.
23. Lautermann J, ten Cate WJ, Altenhoff P, Grümmer R, Traub O, Frank H, Jahnke K and Winterhager E (1998) Expression of the gap-junction connexins 26 and 30 in the rat cochlea. *Cell Tissue Res* **294**, 415–420.
24. Lawrence M (1956) Structures of the spiral prominence and external sulcus and their relation to the organ of corti. *Laryngoscope* **66**, 796–809.
25. Lim DJ (1970) Morphology and function of the interdental cell--an ultrastructural observation. *J Laryngol Otol* **84**, 1241–1256.
26. Liu XZ, Xia XJ, Adams J, Chen ZY, Welch KO, Tekin M, Ouyang XM, Kristiansen A, Pandya A, Balkany T, Arnos KS and Nance WE (2001) Mutations in GJA1 (connexin 43) are associated with non-syndromic autosomal recessive deafness. *Hum Mol Genet* **10**, 2945–2951.
27. Liu YP and Zhao HB (2008) Cellular characterization of Connexin26 and Connnexin30 expression in the cochlear lateral wall. *Cell Tissue Res* **333**, 395–403.
28. McGuirt JP and Schulte BA (1994) Distribution of immunoreactive α- and β-subunit isoforms of Na,K-ATPase in the gerbil inner ear. *J Histochem Cytochem* **42**, 843–853.
29. Mhatre AN, Weld E and Lalwani AK (2003) Mutation analysis of Connexin 31 (GJB3) in sporadic non-syndromic hearing impairment. *Clin Genet* **63**, 154–159.
30. Oesterle EC and Dallos P (1990) Intracellular recordings from supporting cells in the guinea pig cochlea: DC potentials. *J Neurophysiol* **64**, 617–636.

31. Reale E, Luciano L, Franke K, Pannese E, Wermbter G and Iurato S (1975) Intercellular junctions in the vascular stria and spiral ligament. *J Ultrastruct Res* **53**, 284–297.
32. Schulte BA and Adams JC (1989) Distribution of immunoreactive Na^+,K^+-ATPase in gerbil cochlea. *J Histochem Cytochem* **37**, 127–134.
33. Spicer SS and Schulte BA (1991) Differentiation of inner ear fibrocytes according to their ion transport related activity. *Hear Res* **56**, 53–64.
34. Spicer SS and Schulte BA (1997) Golgi-canalicular reticulum system in ion transporting fibrocytes and outer sulcus epithelium of gerbil cochlea. *Anat Rec* **249**, 117–127.
35. Spicer SS and Schulte BA (1998) Evidence for a medial K^+ recycling pathway from inner hair cells. *Hear Res* **118**, 1–12.
36. Spoendlin H (1957) Electron microscopy of Corti's organ in guinea pigs. *Pract Otorhinolaryngol (Basel)* **19**, 192–234.
37. Willingham MC and Rutherford AV (1984) The use of osmium-thiocarbohydrazide-osmium (OTO) and ferrocyanide-reduced osmium methods to enhance membrane contrast and preservation in cultured cells. *J Histochem Cytochem* **32**, 455–460.

Figure Legends

Fig. 1. Light micrographs (a–c) and BSE mode-SEM images (a´–c´) of the rat cochlea obtained in the same portion as a semi-thin section through the modiolus. a, a´: The entire cochlear showing the modiolus (MO), Reissner's membrane (RM), tectorial membrane (TM), organ of Corti (OC), and stria vascularis (SV). b, b´: High magnification images of the spiral ligament in the cochlear middle turn. Claudius cells (CC), outer sulcus cells (OSC), root cells (RC), and the stria vascularis (SV). c, c´: High magnification images of the spiral limb in the middle turn. Inner sulcus cells (ISC) and interdental cells (IDC) are observed more clearly in SEM images than in light micrographs. Scale bar: 300 μm (a, a´), 20 μm (b, c, b´, c´).

Fig. 2. BSE mode-SEM images of serial semi-thin sections (a–f) and 3D reconstruction images (g–i) of root cells in the spinal ligament of the middle turn cochlea. The root cells and the outer sulcus cells (*) are colored pink, with red nuclei. The root cells are connected to each other to form a branched structure like an elaborate tree root in the spiral ligament. SV: stria vascularis; SLg: spiral ligament.

Fig. 3. BSE mode-SEM images of serial semi-thin sections (a–f) and a 3D reconstruction image (g–j) of the spiral limbus in the middle turn. The interdental cells are colored purple and their nuclei are red. The inner sulcus cells are colored light blue and their nuclei blue. The interdental cells are oval or round in shape and are connected to each other to form a comb-shaped network in the spiral limbus. Some connections are also found among the teeth of the comb. The interdental cells just beneath the tectorial membrane extend flat processes to cover the surface of the spiral limbus. Some of the interdental cells are also connected to inner sulcus cells. TM: tectorial membrane; RM: Reissner's membrane.

Fig. 4. TEM images (a–c) of the root cell in the cochlear lateral wall of the middle turn. a: The abutting root cells are interdigitated with irregular projections. b, c: The gap junctions are confirmed

between the root cells and their processes (arrowheads). Scale bar: 2 μm (a), 200 nm (b, c).

Fig. 5. TEM images (a–c) of an interdental cell in the spiral limbs of the middle turn. a: Some interdental cells form a cellular mass by connecting tightly to each other. They also interdigitate with their irregular processes. b, c: Gap junctions (arrowheads) are found between interdigitated processes of inner sulcus cells. Scale bar: 2 μm (a), 200 nm (b, c).

Fig.6. Schematic diagram showing the shape of the root cell cluster and interdental cell network, with the assumption of K^+ circulation occurring in the cochlea. K^+ incorporated into hair cells is circulated to the scala media via the spiral ligament and spiral limbus. The root cell cluster is elaborate in the spiral ligament and intermingled with fibrocytes (type II), suggesting that root cells are important for efficient transfer of K^+ to fibrocytes, using the large surface area of the root cell cluster. The interdental cell network is connected to inner sulcus cells, suggesting that direct K^+ flow into the scala media occurs through this network. SV: stria vascularis; TM: tectorial membrane; SLg: spiral ligament; SLm: spiral limbs; IHC: inner hair cell; OHC: outer hair cell; FC: fibrocyte; RC: root cell; OSC: outer sulcus cell; CC: Claudius cell; HC: Hensen's cell; DC: Deiters' cell; IHC: inner sulcus cell; IDC: interdental cell.

Fig.1.

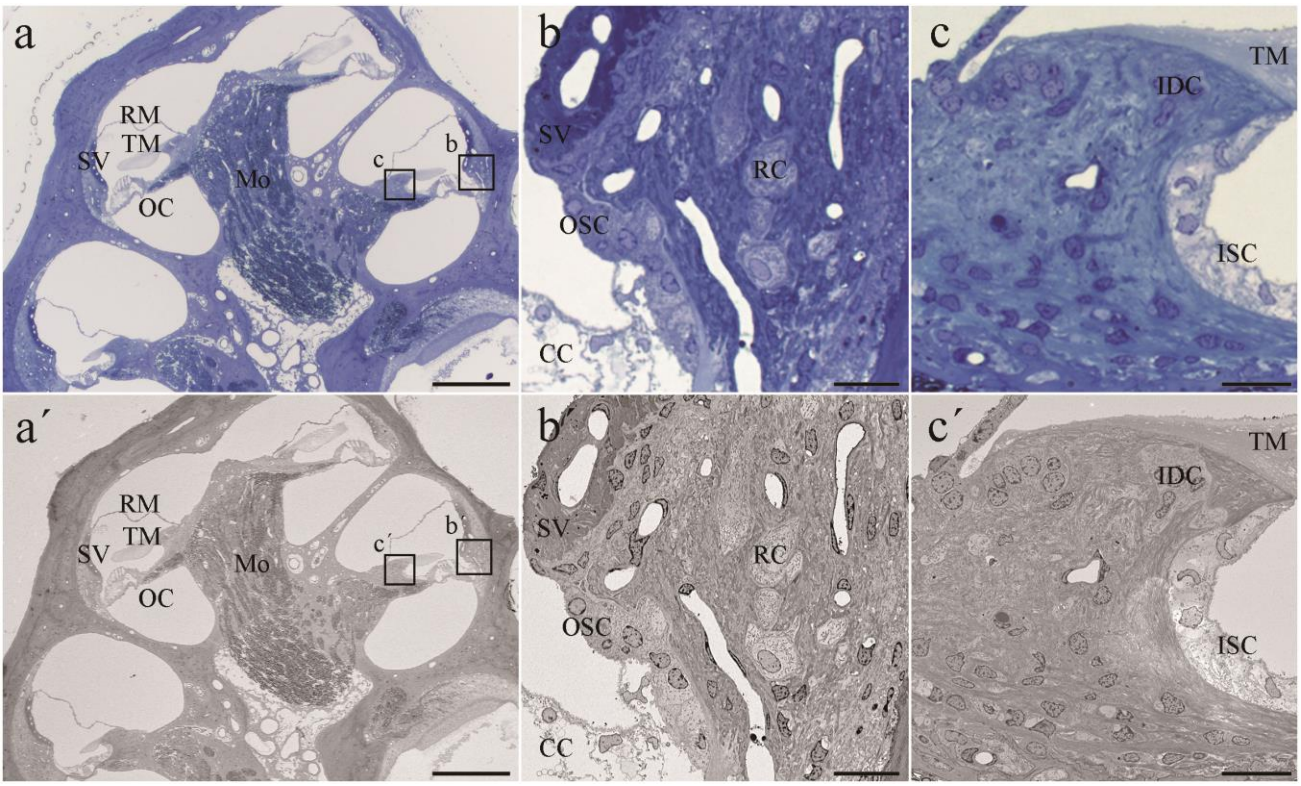
a
RM
TM
SV
Mo
OC
c
b
b
SV
RC
OSC
CC
c
TM
IDC
ISC
a´
RM
TM
SV
Mo
OC
c´
b´
b´
SV
RC
OSC
CC
c´
TM
IDC
ISC

Fig.2.

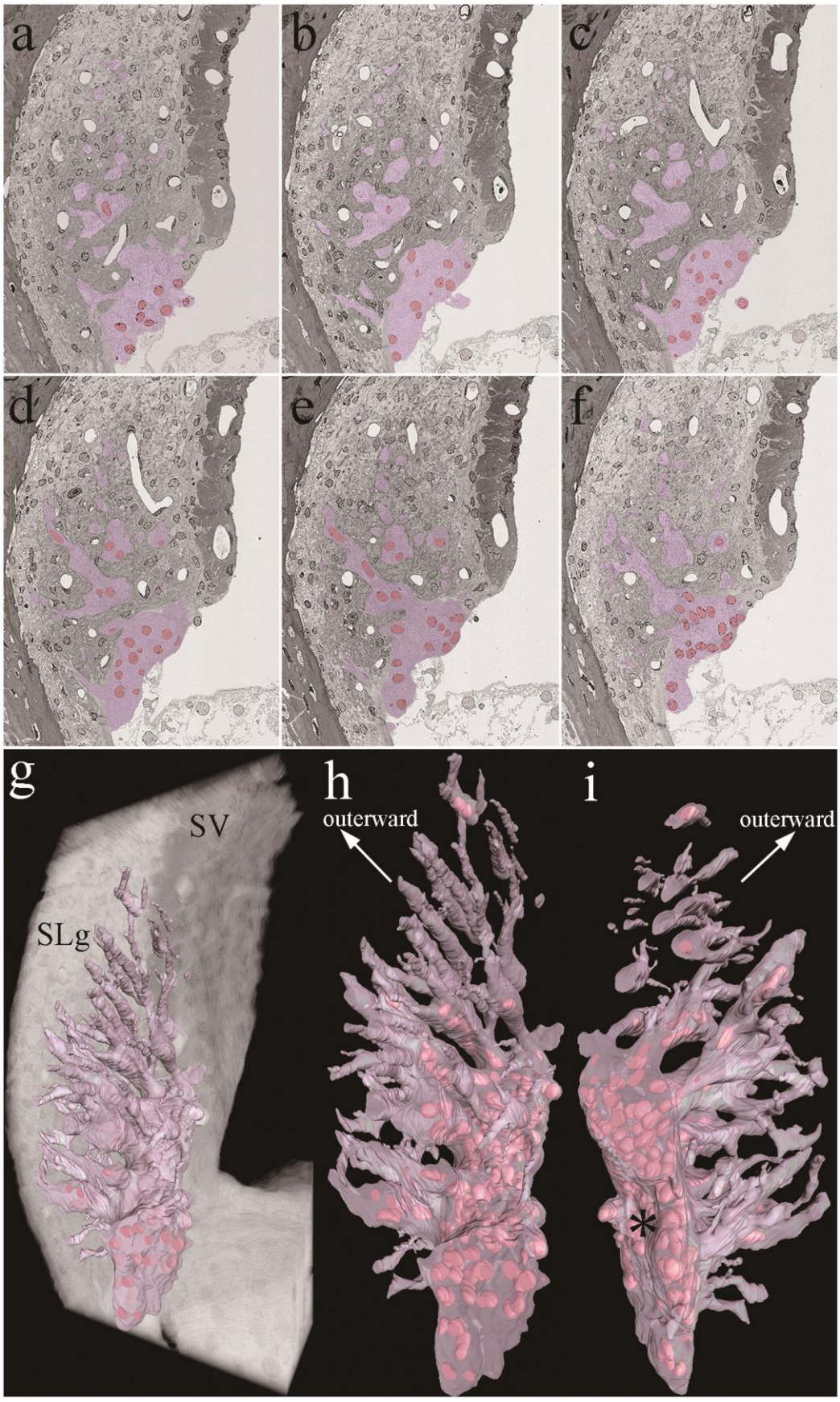

Fig.3.

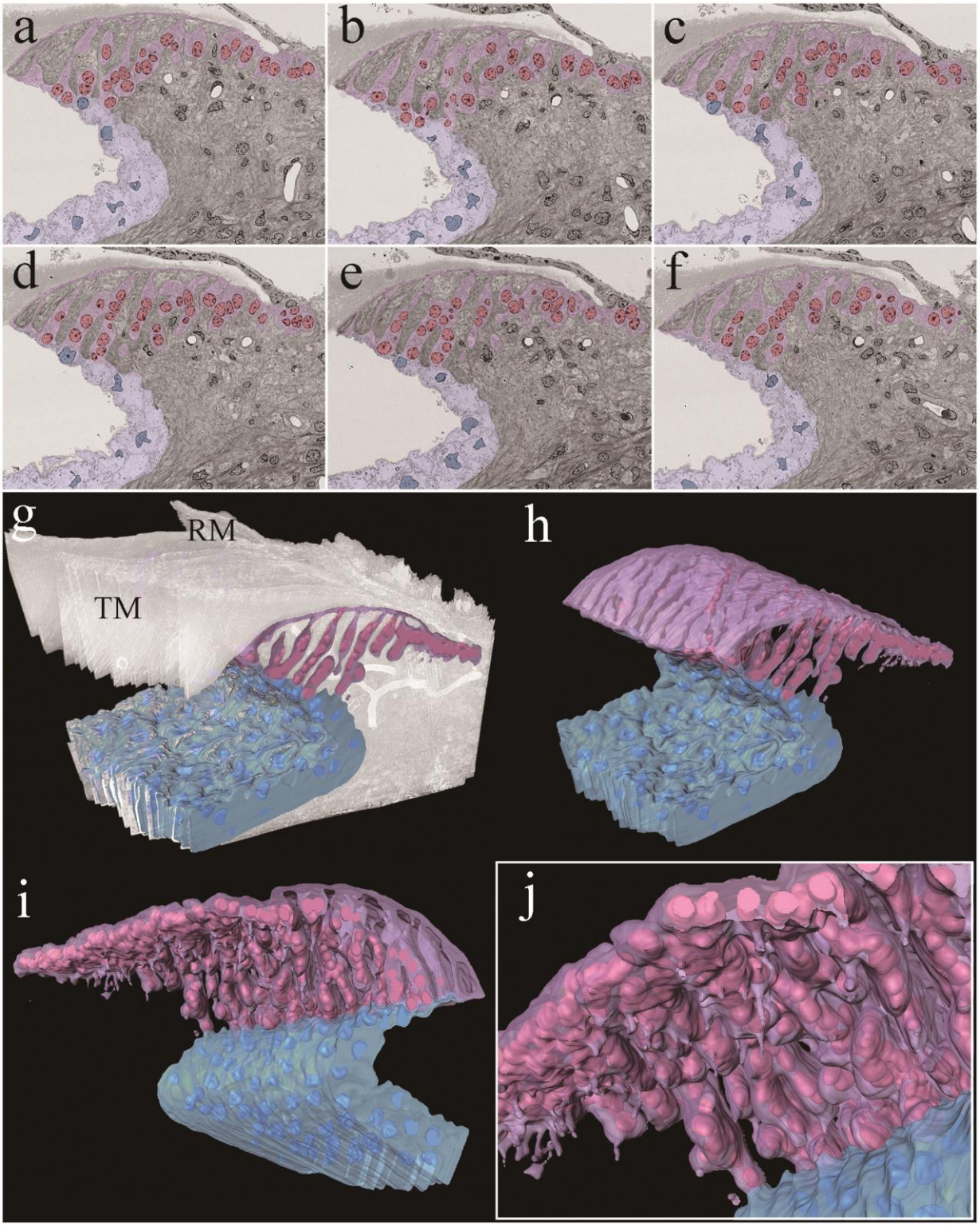

Fig.4.

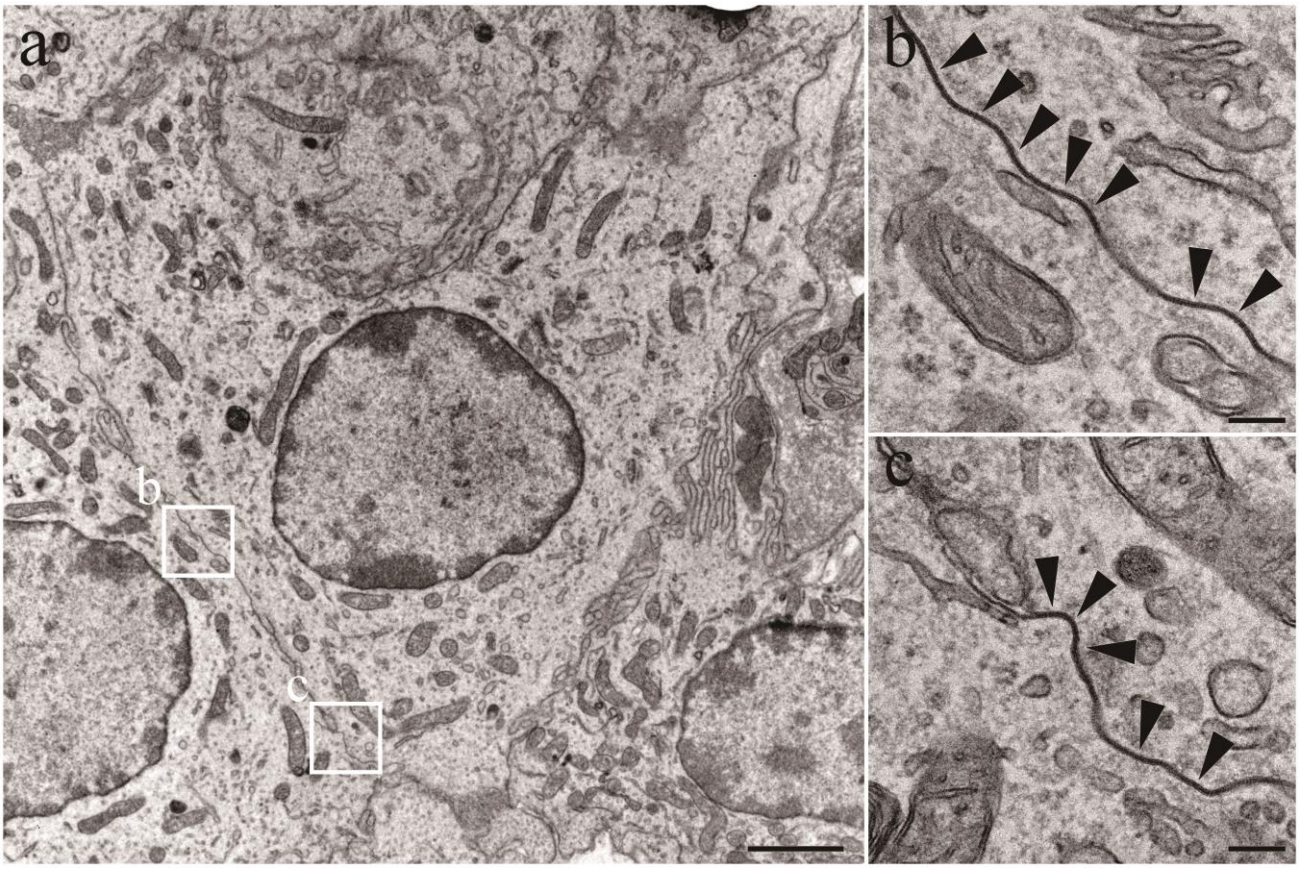

Fig.5.

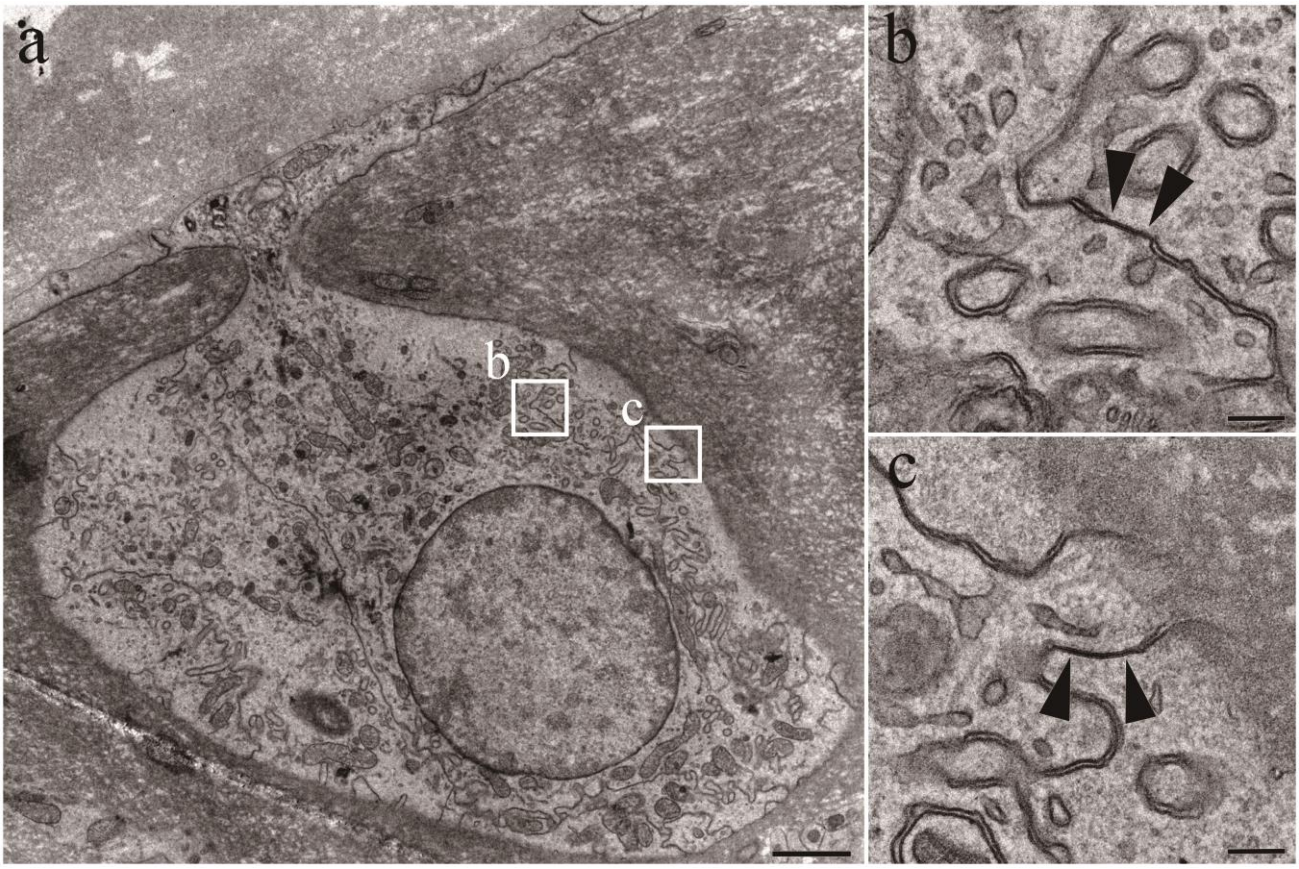

Fig.6.

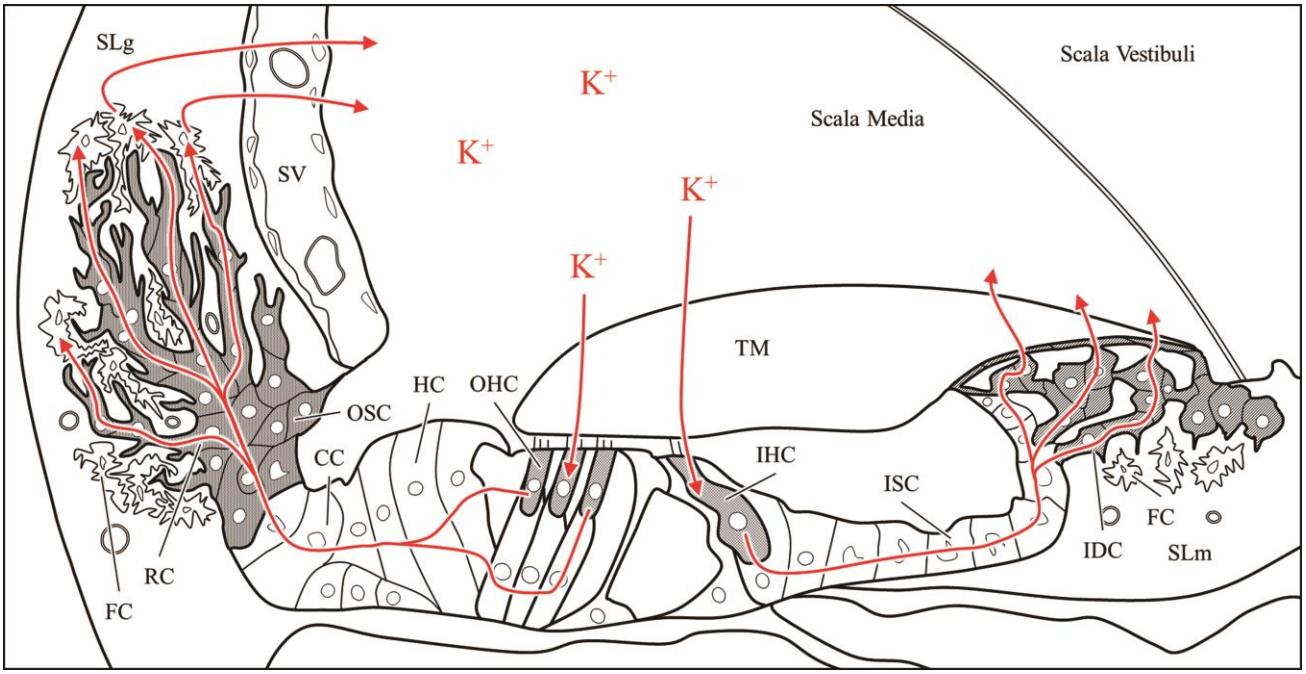
SLg
SV
K+
K+
K+
K+
Scala Vestibuli
Scala Media
TM
HC
OHC
OSC
CC
IHC
ISC
FC
RC
FC
IDC
SLm